Minimum Liquid Fluidization Velocity in Gas-Liquid-Solid Fluidized Beds

L. A. Briens, C. L. Briens, A. Margaritis, and J. Hay
Dept. of Chemical and Biochemical Engineering, The University of Western Ontario, London, Ontario, Canada N6A 5B9

Accurate detection of minimum liquid fluidization is essential to the successful operation of gas-liquid-solid fluidized beds, especially when particle or liquid properties evolve. A gas-liquid-solid system of 3-mm glass beads exhibits three distinct flow regimes as the liquid velocity is increased: compacted, agitated and fluidized-bed regimes. Measurements showed that the bed is not fluidized in the agitated bed regime. Pressure gradient and bed height measurements do not provide the minimum liquid fluidization velocity; instead, they offer the velocity between the compacted and agitated bed regimes. Time-averaged signals are not reliable for determining the minimum liquid fluidization velocity. It can be obtained from the standard deviation, the average frequency, the Hurst exponent and the V statistic of the cross-sectional average conductivity, which can be measured under many industrial conditions.

Introduction

Examples of applications of gas-liquid-solid fluidized bed reactors include coal liquefaction and petroleum hydrotreating. Three-phase fluidization can also be applied to many biological and biochemical processes using immobilized whole cells, subcellular organelles, or enzymes as the solid phase (Fan, 1989; Merchant et al., 1987).

For a gas-liquid-solid fluidized system, the minimum liquid fluidization velocity is the superficial liquid velocity at which the bed becomes fluidized for a given superficial gas velocity. Above the minimum liquid fluidization velocity, there is good contact between the gas, liquid, and solid phases. Concentration and temperature gradients are minimized, which is important if the solid phase is a catalyst, a reactant, or an adsorbent, and if the reaction is endothermic or exothermic as temperature gradients may degrade reaction selectivity, product quality, and catalyst activity.

Several definitions of fluidization have been proposed. Some authors consider that a bed is fluidized when the particles are moving (Ermakova et al., 1970; Fortin, 1984; Lee and Al-Dabbagh, 1978; Nacef, 1991; Nacef et al., 1988; Saberian-Broudjenni et al., 1984, 1987). A second definition considers a three-phase bed as fluidized when the gas-liquid-solid mixture assumes the macroscopic properties of a homogeneous fluid. The bed hydrostatic pressure drop can then be directly related to the average density of the gas-liquid-solid mixture. This article uses the second definition.

Continuous monitoring of the fluidization regime is required if phase properties evolve during the process. For example, with biological and biochemical processes, the gas and liquid properties change as the immobilized cells, organelles, or enzymes consume dissolved gases and nutrients in the liquid and produce gases and surfactants. The apparent particle density may also decrease as gaseous byproducts become trapped in the immobilization matrix.

Bed-pressure measurements or visual observations have generally been used to measure the minimum liquid fluidization velocity. For liquid-solid fluidization, a plot of the pressure drop through the bed or the pressure gradient within the bed vs. superficial liquid velocity displays two linear regions whose intersection corresponds to the minimum liquid fluidization velocity. Although some researchers apply these techniques to gas-liquid-solid systems (Begovich and Watson, 1978; Costa et al., 1986; Jean, 1988; Song et al., 1989; Zhang et al., 1995), other researchers rely on visual observations. Visual observations determine the minimum liquid fluidization velocity as either the velocity at which the bed first begins to expand or as the velocity at which any particle within the bed continuously shifts position with neighboring particles (Ermakova et al., 1970; Fortin, 1984; Lee and Al-Dabbagh, 1978; Nacef, 1991; Nacef et al., 1988; Saberian-Broudjenni et al., 1984, 1987).

Correspondence concerning this article should be addressed to C. L. Briens.

Table 1. Summary of Literature on Minimum Fluidization Velocity

Reference	Exper. Technique	Particles	d_p or d_e (mm)	ρ_p (kg/m^3)	Liquid	Gas	Correlation
Begovich and Watson (1978)	Pressure Drop	Alumina Alumino-Silicate Plexiglas Glass	6.2 1.9 6.3 4.6, 6.2	1,990 1,720 1,170 2,240, 2,200	Water	Air	$R_{Lmf} = 5.121\times10^{-3} Ar^{0.662} Fr^{-0.118}$ $U_g \neq 0$ $\frac{U_{Lmf}}{U_{Lmf}^{LS}} = 1 - 1{,}622 U_g^{0.436} \mu_L^{0.227} d_p^{0.598} \times(\rho_p - \rho_L)^{-0.305}$ $U_g \to 0$
Costa et al. (1986)	Pressure to Find Bed Height	Glass, Aluminum, and Benzoic Acid Covered with Paint Film	3–5.9 ($\phi = 0.87$–1)	1,200–2,700	Water CMC Solutions	Air CO_2 He Me	$U_{Lmf} = 6.969\times10^{-4}\, U_g^{-0.328} \times(\phi d_p)^{1.086}(\rho_p - \rho_L)^{0.865} D_c^{0.042} \mu_L^{-0.355}$
Jean (1988)	Pressure Gradient	Glass	0.330, 0.460, 0.778, 1.0, 3.04, 3.99, 6.11	2,200–2,876	Water	Air	
Song et al. (1989)	Pressure Drop	Catalysts	1.67 ($\phi = 0.72$) 1.85 ($\phi = 0.69$) 1.56 ($\phi = 0.78$) 1.51 ($\phi = 0.75$) 1.69 ($\phi = 0.71$) 1.57 ($\phi = 0.74$) 1.90 ($\phi = 0.68$)	1,890 2,000 2,000 1,890 1,890 2,000 2,000	Water Water + 0.5% *t*-pentanol	Air	$\frac{U_{Lmf}}{U_{Lmf}^{LS}} = 1 - 376 U_g^{0.327} \mu_L^{0.227} d_e^{0.213} \times(\rho_p - \rho_L)^{-0.423}$
Zhang et al. (1995)	Pressure Gradient	Sand Steel Shot TFE Coated Glass Glass Glass	2.4 ($\phi = 0.8$) 1.2 2.5 1.5, 2.5 3.7, 4.5	2,610 7,510 2,520 2,530, 2,520 2,510, 2,490	Water	Air	
Ermakova et al. (1970)	Visual	Glass	0.6–2.0	Not specified	Water Water + 15% Glycerine Water + 50% Glycerine	Air	$\frac{U_{Lmf}}{U_{Lmf}^{LS}} = 1 - \epsilon_g - 0.5 U_g^{0.075}$
Fortin (1984)	Visual	Alumina Alumina Alumina Alumina + Ce	1.6–2.84 2.0 ($\phi = 0.78$) 1.8 ($\phi = 0.82$) 1.66	1,330–2,000 2,000 2,000 2,500	Cyclohexane	N_2	$U_{Lmf} = 0.427 U_g^{-0.198} d_p^{1.539} (\rho_p - \rho_L)^{0.775}$ valid for: $U_g > 1$ cm/s, $1.6 \le d_p \le 2.84$ mm, $550 \le \rho_p - \rho_L \le 1{,}720$ kg/m^3
Lee and Al-Dabbagh (1978)	Visual	Glass	4.03, 6.08	2,560, 2,590	Not Specified	Not Specified	
Nacef (1991)	Visual	Polypropylene Polypropylene Glass	2.1 ($\phi = 0.82$) 3.1 ($\phi = 0.87$) 1.2, 2, 3.1, 4	1,350 1,700 2,525	Water Water + 0.5% Ethanol Water + 1% Ethanol Water + 2% Ethanol Water + 64 g/l NaCl Water + 0.5% *n*-pentanol Water + 1% *n*-pentanol Water + 0.5% *t*-pentanol Water + 1% *t*-pentanol Perchloroethylene	N_2	$\frac{U_{Lmf}}{U_{Lmf}^{LS}} = \exp(-13.8 Fr^{0.35} (\rho_p - \rho_L)^{-0.38})$ only valid for water
Saberian-Broudjenni et al. (1987)	Visual	Alumina Alumina Alumina Alumina Alumina Glass	1.74 1.87 2.55 2.0(ϕ=0.71–0.78) 1.8($\phi = 0.82$) 1.37, 3.18	1,515–2,150 1,420–2,100 1,380–2,015 1,600–2,160 1,600–2,160 2,640, 2,190	Water Kerosene Cyclohexane Gas Oil C_2Cl_4	CO_2 He N_2	
Saberian-Broudjenni et al. (1984)	Visual	Alumina Alumina Glass	2.55, 2.9 2.15 ($\phi = 0.87$) 1.37, 3.18	1,380–2,300 1,590–2,145 2,640, 2,190	Water Kerosene Cyclohexane, C_2Cl_4	CO_2 He N_2	

Table 1 summarizes previous research on the minimum liquid fluidization velocity in gas-liquid-solid systems. Ar is the Archimedes number ($Ar = d_p^3 \rho_L(\rho_p - \rho_L)\, g/\mu_L^2$). d_e is effective particle diameter, d_p is particle diameter (m), R_{Lmf} is the Reynolds number at minimum liquid fluidization velocity ($R_{Lmf} = U_{Lmf} d_p \rho_L/\mu_L$), Fr is Froude number ($Fr = U_g/gd_p$), U_g is superficial gas velocity (m/s), U_{Lmf} is minimum liquid fluidization velocity for a three-phase system (m/s), U_{Lmf}^{Ls} is minimum liquid fluidization velocity for a liquid-solid system (m/s). ρ_p is solids density (kg/m^3), ρ_L is liquid density (kg/m^3), μ_L is liquid viscosity (kg/ms), and ϕ is particle sphericity. Many studies have been conducted with water and

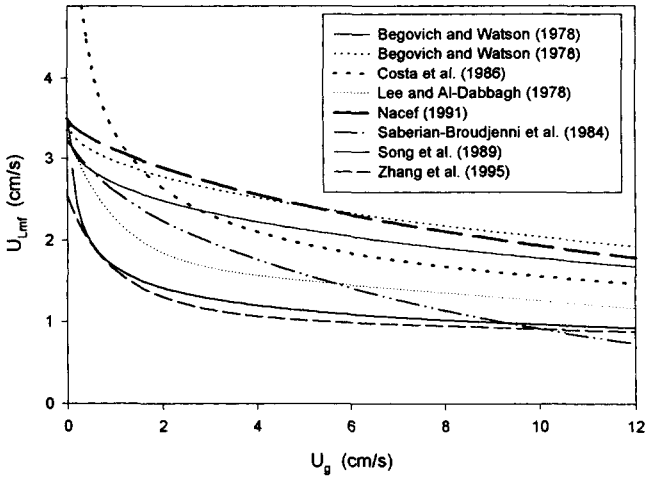

Figure 1. Minimum liquid fluidization velocities reported in the literature.

glass beads in the mm range. Figure 1 then compares the results for 3 mm glass beads fluidized by water and air using interpolation or extrapolation where correlations had not been developed. For a given superficial gas velocity, a wide range of minimum liquid fluidization velocities has been reported. Although some of this variation may result from differences in gas distribution, most of it can probably be attributed to subjective visual observations or bias from the experimental method.

The first objective of this article is to draw upon a variety of measurements, in addition to the standard pressure measurements and visual observations, to clearly characterize flow regime transitions. The second objective is to identify simple, reliable techniques to measure the minimum liquid fluidization velocity in a gas-liquid-solid system. Special emphasis is placed on techniques suitable for pilot- and industrial-scale units.

Equipment and Experimental Methods

Fluidized-bed column

The Plexiglas fluidized-bed column was 2 m high and 0.1 m in diameter (Figure 2). The liquid flow rate was measured with calibrated rotameters, and the gas flow rate was regulated by a bank of four sonic nozzles in parallel. The gas and liquid streams merged and passed through a shutoff valve, an expansion cone, a mixing section containing ceramic saddles, and a 3-mm thick perforated grid with 180, 2-mm-dia. holes before entering the bed. The mixing section and the grid ensured that the gas and liquid were well mixed and evenly distributed into the bed. A cylindrical screen at the top of the column allowed gas to escape and liquid to be recirculated while retaining any entrained particles.

The gas was oil-free air and the liquid was an aqueous solution of 1 wt. % Na_2HPO_4 maintained at 25 ± 0.3°C by a heat exchanger in the liquid recirculation tank. Spherical 3 mm glass beads with a density of 2,471 kg/m^3 were selected as the solids to facilitate comparison with other published studies.

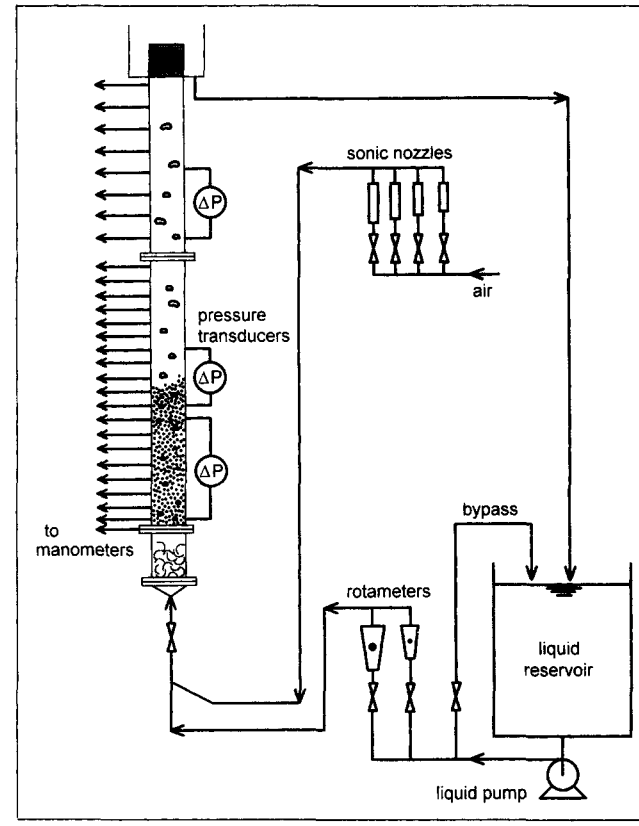

Figure 2. Experimental equipment.

Pressure measurements

The column was equipped with 28 pressure taps, installed along the wall of the fluidization section, connected to a pressurized liquid manometer system. Differential pressure transducers were also installed to measure pressure gradients within the bed, across the bed surface, and within the freeboard (see Figure 2).

Bed height measurements

At low liquid velocities, an average bed height could be estimated by visual observations or from manometer readings as a plot of pressure vs. height above the grid shows two regions which intersect at the average bed height. At high superficial liquid velocities, the average bed height was obtained from pressure gradients within the bed, across the bed surface, and within the freeboard measured using the pressure transducers.

Conductivity measurements

The bed-average conductivity was measured using two diametrically opposed wall electrodes 10 cm and 50.5 cm above the grid. The cross-sectional average conductivity within the bed was measured using two diametrically opposed wall electrodes both located 30 cm above the grid. The electrodes were 1 cm by 6 cm rectangles of platinized titanium mesh.

Local conductivity measurements were performed by inserting a probe into the column through pressure taps 31 cm and 36 cm above the grid. The probe consisted of two stain-

less steel rods 4.8 mm in diameter and 18 cm in length. A thin coating of Rilsan (from Elf Atochem) was used as an insulator leaving exposed areas of 1 cm in length at each end of the rods. The rods were in the same vertical plane with their tips aligned at the same radial position.

For all conductivity measurements, a sine wave alternating current of 5 V and 2,500 Hz was applied. The data acquisition frequency was 500 Hz.

Liquid backmixing measurements

Calibration experiments verified that the conductivity of the 1 wt. % Na_2HPO_4 solution increased linearly with temperature. Salt solution at about 90°C was injected with a sparger into the bed at 30 mL/s for 70 s; visual observations confirmed that the injection did not induce local fluidization. The stainless steel sparger with 4.57 mm ID and equipped with ten alternating 1-mm-dia. holes was inserted into the bed 25 cm above the grid. The sparger holes were equally spaced across the column diameter and aligned for horizontal liquid injection. An alternating current of 3 V and 60 Hz was applied to two sets of 1 cm by 6 cm rectangular platinized titanium wall electrodes mounted inside the column at diametrically opposed locations 5 cm below and 5 cm above the sparger. The cross-sectional average conductivity before and during the hot solution injection was determined by measuring the voltage drop across 100 Ω resistances at a frequency of 100 Hz.

Measured conductivities were used to calculate a backmixing index which was defined as:

$$\text{Backmixing Index} = \frac{\left[\dfrac{(\gamma_{\text{during injection}} - \gamma_{\text{before injection}})}{\gamma_{\text{during injection}} + \gamma_{\text{before injection}}}\right]_{\text{5 cm below sparger}}}{\left[\dfrac{(\gamma_{\text{during injection}} - \gamma_{\text{before injection}})}{\gamma_{\text{during injection}} + \gamma_{\text{before injection}}}\right]_{\text{5 cm above sparger}}} \quad (1)$$

where γ is conductivity (mho). No backmixing would give an index of zero and perfect backmixing an index of one.

Bubble probe measurements

The bubble conductivity probe consisted of two 0.5-mm-dia. stainless steel needles insulated and anchored 1 mm apart by a nylon plug encased in a 4.8-mm-dia. hollow stainless steel tube. The needles extended 4 mm beyond the plug (Hudson, 1996). The probe was located 35 cm above the grid with the needles aligned in the horizontal plane. A sine wave alternating current of 5 V and 2,500 Hz was applied to the bubble probe with a data acquisition frequency of 500 Hz.

Phase holdup measurements

The average solids holdup was obtained from the mass of solids introduced into the column and the measured bed height

$$\epsilon_s = \frac{4M_s}{\rho_p \pi D_c^2 H_{\text{bed}}} \quad (2)$$

where D_c is column diameter (m), M_s is the mass of solids (kg), H_{bed} is the bed height (m), and ϵ_s is the solids holdup. The average liquid holdup within the bed was obtained from the cross-sectional average conductivity after calibration. The average gas holdup within the bed was calculated from the solids and liquid holdup

$$\epsilon_g = 1 - \epsilon_s - \epsilon_L \quad (3)$$

where ϵ_g is gas holdup and ϵ_L is liquid holdup. Bubble probe measurements at 17 radial locations showed a nearly flat radial profile in the fluidized regime. A flat radial profile of the liquid holdup was also obtained with the local conductivity probe. There was therefore a nearly flat radial profile of all three holdups in the fluidized regime.

The measured gas and liquid holdups were verified by disengagement experiments. The gas holdup in the freeboard was calculated from manometer readings. The gas and liquid feeds were then simultaneously shut off. The bed height, the liquid level in the column, and the mixing zone, below the grid, were measured. To determine the volume of gas trapped within the bed, the liquid was drained, weighed and then slowly reintroduced into the bed using a sparger. The liquid front moved slowly through the bed displacing the gas.

Experimental Results and Discussion

Visual observations

For a fixed superficial gas velocity, as the liquid velocity was decreased three regimes were observed:

- *Fluidized Bed.* At high liquid velocities, the bed was well fluidized. Particles anywhere in the bed continuously shifted position with each other.
- *Agitated Bed.* As the liquid velocity was decreased, a radical change in bed hydrodynamics was observed. There was no longer smooth, continuous motion of the bed particles. Instead, particles were moved intermittently by the gas bubbles. The bed was said to be in the agitated bed regime.
- *Compacted Bed.* At low liquid velocities, the particles formed a uniform close-packed structure. The particles exhibited small agitated movements with no net vertical or horizontal displacement. The transition velocity between the agitated and the compacted bed was denoted as the minimum agitation velocity U_{Lma} (m/s).

The three regimes were also observed when the liquid velocity was increased from the compacted bed state. Regime transitions occurred at about the same liquid velocities.

Although many researchers have studied minimum liquid fluidization in gas-liquid-solid systems using monosize spherical glass beads, only Lee and Al-Dabbagh (1978) and Saberian-Broudjenni et al. (1987) have reported the organization of the particles into a uniform close-packed structure at low liquid velocities. Fortin (1984) reported a transition regime between the fixed and fluidized beds wherein the particles begin to move randomly, and Saberian-Broudjenni et al. (1984) reported a transition state attributed to progressive fluidization from the top of the bed downwards.

Some analogy may be drawn with mechanically vibrated gas-solid beds. External vibration or agitation of the bed at certain frequencies has been found to improve fluidization of

cohesive solids. At low frequencies, however, the bed can become compacted increasing the velocity of incipient fluidization (Nowak et al., 1993). If the agitation provided by the gas and the liquid flow through the bed can be compared to that externally applied to a gas-solid bed, then it is expected that a compacted bed could be formed. Power spectrum analysis of conductivity and bubble probe measurements taken in the experimental three-phase system verified that approximately 50% of the power was for frequencies less than 3.5 Hz.

Liquid backmixing

Since visual observations indicated that the three regimes exhibited very different solids movement, solids backmixing could be used to measure the transition velocities. Fortin (1984) used a ferromagnetic solids tracer to measure solids mixing times in a three-phase fluidized bed. As the measurement technique was difficult, limited data was acquired and solids backmixing in the reported transition regime was not confirmed. Since liquid and solids flow patterns are related, the more easily performed liquid backmixing measurements were used for this study.

Figure 3 is a plot of the previously defined backmixing index (Eq. 1) vs. superficial liquid velocity at a superficial gas velocity of 6 cm/s. The three regimes were identified using straight lines fitted by minimizing the sum of squared differences between experimental values and values calculated with the straight line equations. Above a superficial liquid velocity of 2.26 cm/s, the bed was fluidized and the backmixing index increased, which indicated increasing liquid backmixing. Between superficial liquid velocities of 0.87 and 2.26 cm/s, the low backmixing index indicated minimal liquid backmixing. This range corresponds to the agitated bed regime characterized by slow vertical displacement of particles. Below a superficial liquid velocity of 0.87 cm/s, the backmixing index increased. Measurements with the bubble probe indicated that below this velocity, the gas bubbles were concentrated at the center, which lowered the density of the gas-liquid mixture and induced liquid circulation.

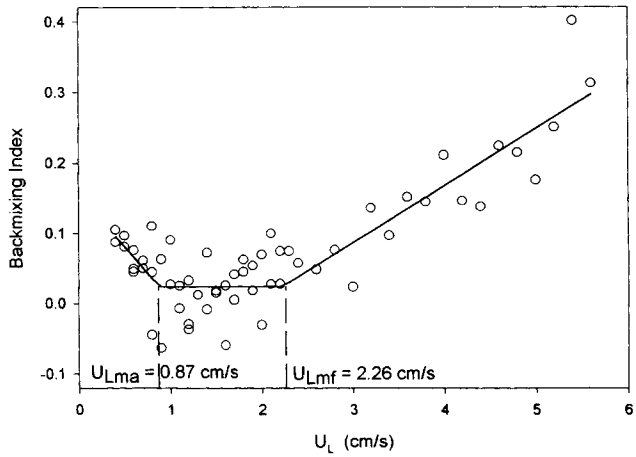

Figure 3. Backmixing index as a function of superficial liquid velocity for a superficial gas velocity of 6 cm/s.

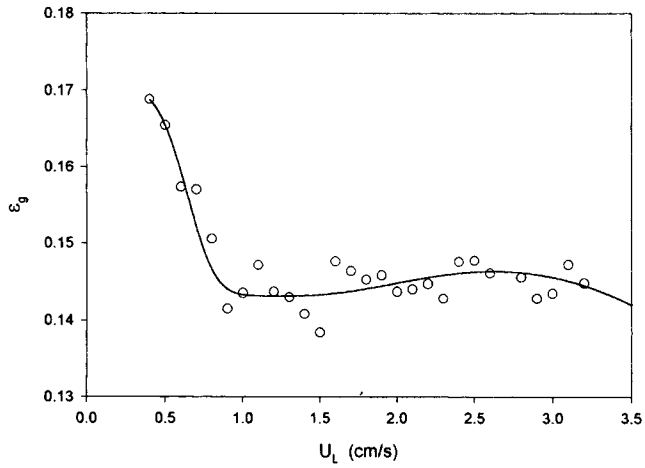

Figure 4. Average gas holdup within the bed for a superficial gas velocity of 6 cm/s.

Phase holdups

Figure 4 shows the gas holdup as a function of superficial liquid velocity for a superficial gas velocity of 6 cm/s. For liquid velocities above 1 cm/s, the gas holdup was approximately constant. Figure 5 shows the liquid holdup at a superficial gas velocity of 6 cm/s. Allowing for measurement errors, the results from the disengagement technique support the values from the cross-sectional average conductivity. The results also agree with those obtained by Nacef et al. (1988) under similar conditions, using another variation of the disengagement technique.

When a bed is fluidized, the bed pressure gradient equals the product of the bed density with gravitational acceleration

$$\left(-\frac{\Delta P}{\Delta z}\right)_{\text{bed}} = \rho_{\text{bed}} g = (\rho_L \epsilon_L + \rho_p \epsilon_s) g \qquad (4)$$

where $\Delta P/\Delta z$ is pressure gradient (Pa/m), and ρ_{bed} is bed density (kg/m^3). Figure 6 compares the measured bed pres-

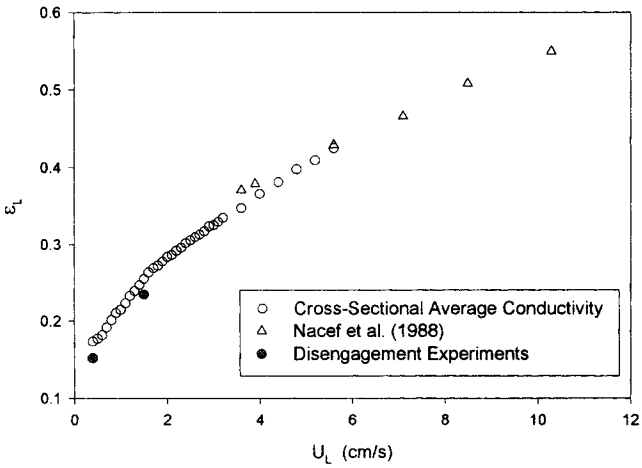

Figure 5. Average liquid holdup within the bed for a superficial gas velocity of 6 cm/s.

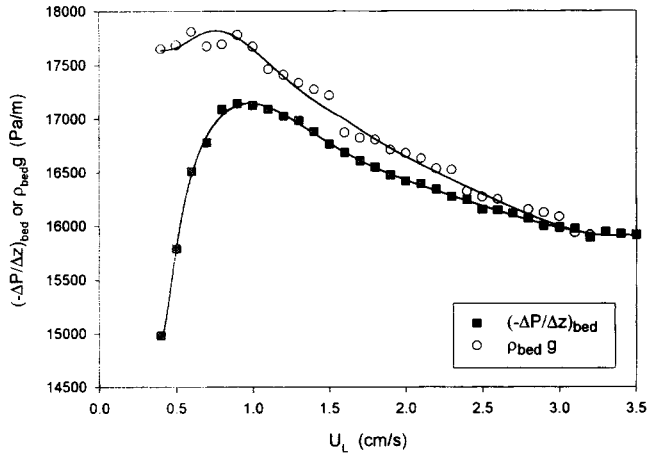

Figure 6. Bed pressure gradient and the product of the bed density with gravitational acceleration as a function of superficial liquid velocity for a superficial gas velocity of 6 cm/s.

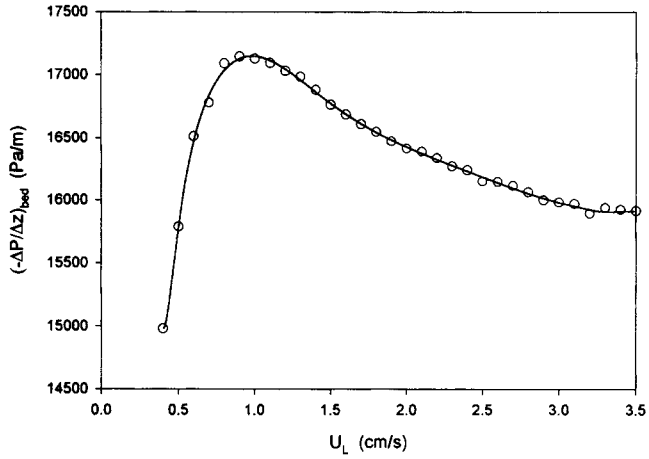

Figure 8. Bed pressure gradient for a superficial gas velocity of 6 cm/s.

sure gradient to the product of the bed density with gravitational acceleration which was obtained from the measured phase holdups. The product of the bed density with gravitational acceleration becomes equal to the bed pressure gradient at superficial liquid velocity of approximately 2.4 cm/s. This confirms the visual observations and liquid backmixing results. In the agitated bed regime, roughly between 0.9 and 2.3 cm/s, the bed is not fluidized.

At the fixed to agitated bed regime transition, the measured bed porosity was 0.36. Dullien (1984) reports porosities from 0.36 to 0.38 for beds of monosize spheres compacted by vibration. This confirms that the gas bubbles act to compact the bed.

Techniques for detection of minimum liquid fluidization

Detection from Time-Averaged Signals. The detection of the minimum liquid fluidization velocity was first attempted using the time-averaged signals.

For the liquid-solid system, the minimum liquid fluidization velocity was determined to be 3.5 cm/s from pressure gradient measurements (Figure 7). This was confirmed by visual observations and comparison with correlations from the literature (Grace, 1982). For the gas-liquid-solid system, a plot of the pressure gradient within the bed vs. superficial liquid velocity showed a distinct maximum (Figure 8).

Figure 9 shows that the superficial liquid velocities corresponding to the maximum pressure gradients agree well with minimum liquid fluidization values interpolated from Zhang et al. (1995). Visual observations and liquid backmixing measurements, however, indicate that these velocities correspond to the transition between the fixed and agitated bed regimes. As shown earlier, the bed is not fluidized in the agitated bed regime.

Figure 10 shows that for a superficial gas velocity of 6 cm/s, the bed height steadily increased at liquid velocities higher than 0.9 cm/s. This velocity corresponds to the minimum agitation velocity.

In Figures 11–15 to eliminate any bias all data above the minimum agitation velocity were fitted with straight lines by minimizing the sum of squared differences between experi-

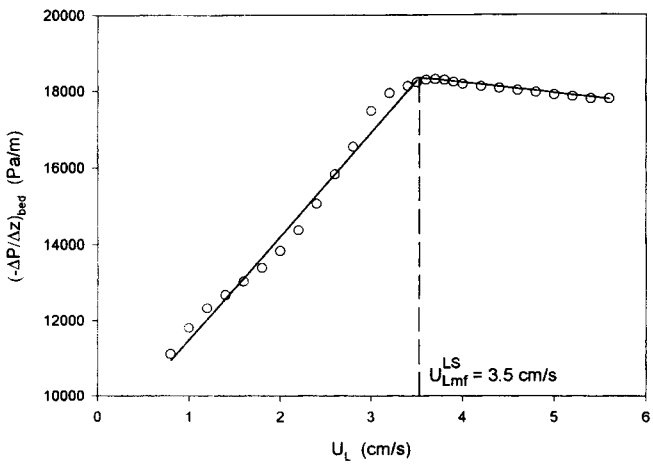

Figure 7. Pressure gradient within the liquid-solid bed.

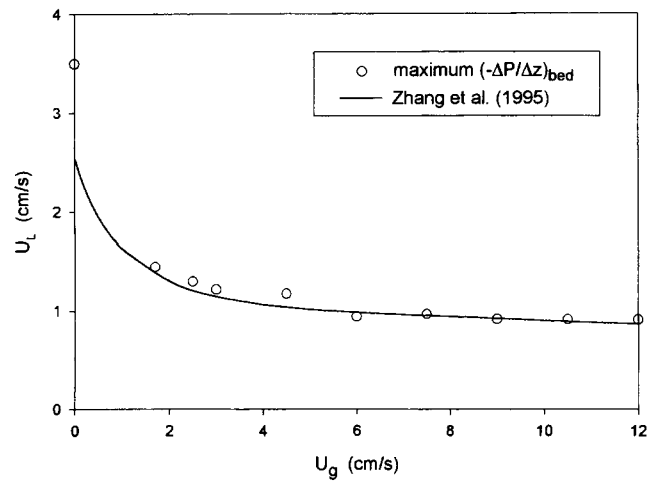

Figure 9. Maximum bed pressure gradient vs. minimum liquid fluidization velocities of Zhang et al. (1995).

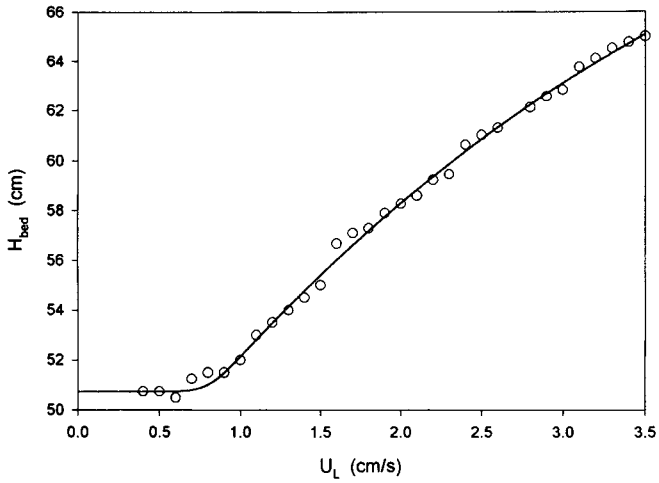

Figure 10. Variation of bed height with liquid velocity at a superficial gas velocity of 6 cm/s.

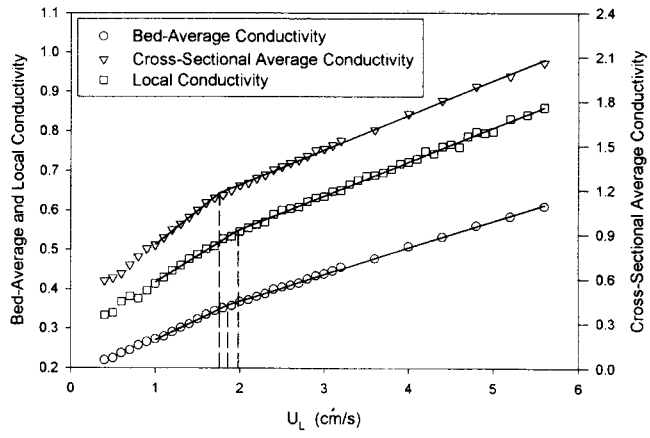

Figure 11a. Variation of conductivity measurements with liquid velocity at a superficial gas velocity of 6 cm/s.

Local conductivity probe at $r = 0$ cm.

mental values and values calculated with the straight line equations. Although the results are only shown at selected superficial gas velocities, similar analyses were performed on all data.

Figure 11 shows the various conductivity measurements and the bubble probe response at two radial positions. A transition at a superficial liquid velocity around 2 cm/s can be seen although less clearly with the conductivity measurements (Figure 11a) than with the bubble probe measurements (Figure 11b). At gas velocities well below 6 cm/s, however, the transition becomes very difficult to detect.

Even under well-controlled laboratory conditions, the time-averaged values were not very reliable for determining the minimum liquid fluidization velocity. They are therefore unsuitable for industrial applications.

Detection from Signal Fluctuations. Four different approaches were attempted using the standard deviation of the signal, its average frequency, its Hurst exponent, and a V statistic derived from Hurst's analysis.

The transition was sharper with the standard deviation of conductivity (Figure 12a) than with the time-averaged conductivity (Figure 11a). (r = radial position, cm ($r < 0$ cm indicates that the probe extended less than 5 cm from the wall into the column; $r = 0$ cm corresponds to the column central position).) It could also be detected from the standard deviation of the bubble probe response (Figure 12b). In addition, the transition was observed with the standard deviation of the pressure gradient within the bed and across the bed surface (Figure 12c). Figure 12 shows the transition was sharp using the standard deviation of all measurements at a superficial gas velocity of 6 cm/s. At higher gas velocities, the transition remained clear. At lower gas velocities, however, only the cross-sectional average and local conductivity measurements showed a clear transition. The rest of this section considers only the cross-sectional average conductivity which would be easier to measure under industrial conditions.

A sharp transition at the minimum liquid fluidization velocity was observed when the average frequency of the cross-sectional average conductivity was plotted as a function of liquid velocity. Figure 13 shows the transition at a superficial

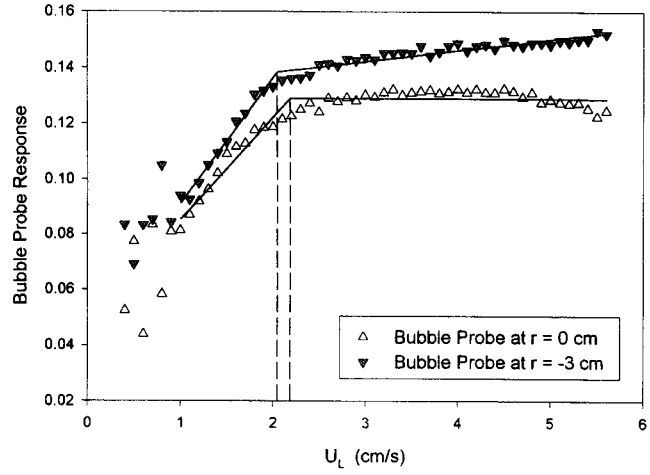

Figure 11b. Variation of bubble probe response with liquid velocity at a superficial gas velocity of 6 cm/s.

gas velocity of 1.7 cm/s. The transition was clear at both high and low gas velocities.

Hurst (1951) invented a new method of analysis for time series of natural phenomena. A time series can be characterized by its Hurst exponent which is always between 0 and 1. For a random walk process such as Brownian motion, there is no correlation between past and future increments and the exponent is 0.5. An exponent greater than 0.5 indicates persistence in the data, that is, the trend in the time series, whether increasing or decreasing, will likely continue. An exponent less than 0.5 indicates antipersistence in the data, that is, the trend will likely reverse itself.

Briens et al. (1997) applied Hurst's analysis to signals from various probes in gas-liquid-solid beds. They found that, in all cases, there were two frequency regions over which a well defined, stable Hurst exponent could be obtained. The low frequency exponent was obtained at frequencies of 0.15 to 0.5 Hz, and the high frequency exponent was obtained at frequencies of 15 to 50 Hz. The low frequency exponent,

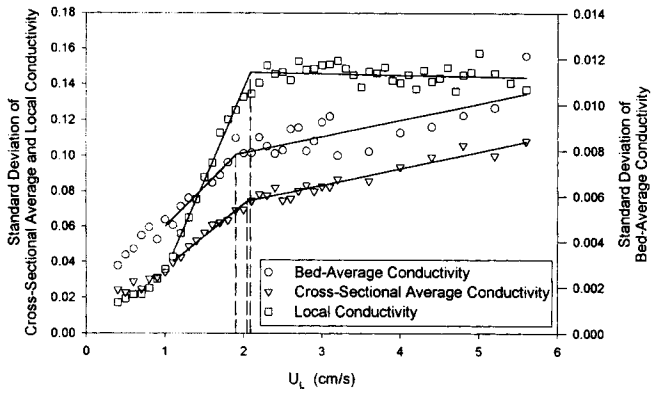

Figure 12a. Variation of the standard deviation of conductivity measurements with liquid velocity at a superficial gas velocity of 6 cm/s.

Local conductivity probe at $r = 0$ cm.

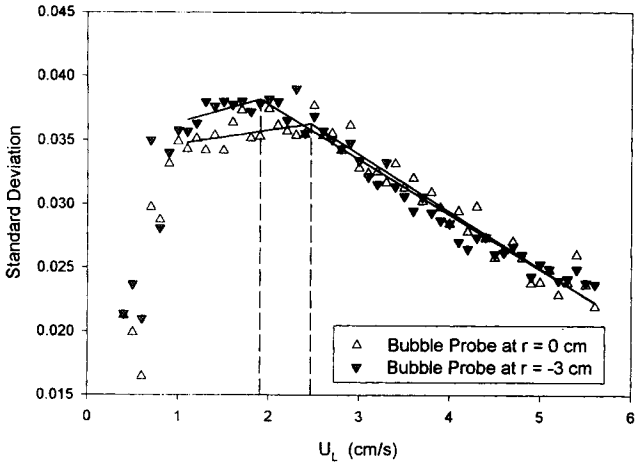

Figure 12b. Variation of the standard deviation of bubble probe response with liquid velocity at a superficial gas velocity of 6 cm/s.

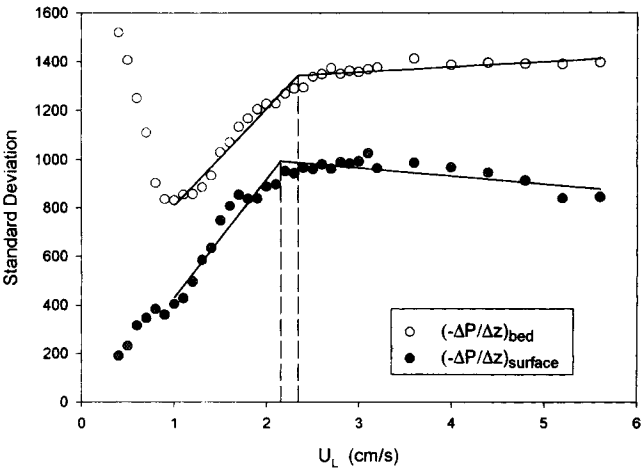

Figure 12c. Variation of the standard deviation of the pressure gradient within and across the bed surface with liquid velocity at a superficial gas velocity of 6 cm/s.

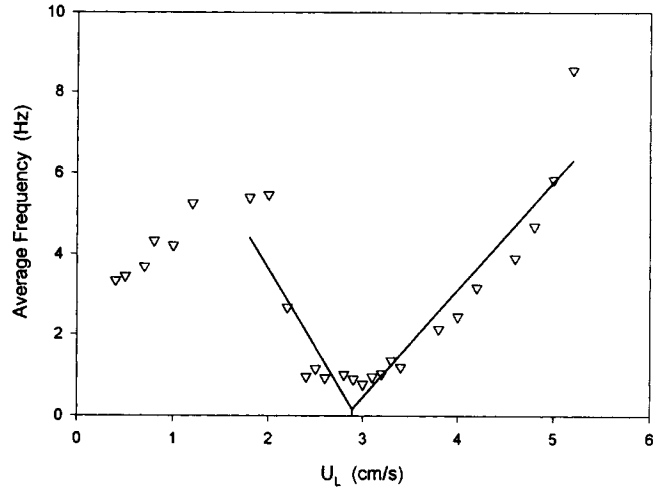

Figure 13. Average frequency of the cross-sectional average conductivity signal at a superficial gas velocity of 1.7 cm/s.

however, could not be determined as accurately as the high frequency exponent. Therefore, although two frequency regions were also found in this study, only the high frequency exponent was used. As shown in Figure 14, using a superficial gas velocity of 1.7 cm/s as an example, a clear transition at the minimum liquid fluidization velocity was obtained with the high frequency Hurst exponent.

The V statistic is obtained from Hurst's analysis. It was proposed by Hurst (1951) to measure the strength of the cyclic, nonperiodic behavior of a time series. Briens et al. (1997) found that the maximum of the V statistic provided detection of gas maldistribution. Figure 15 shows that the V statistic also allows detection of the minimum liquid fluidization velocity from the cross-sectional average conductivity.

The minimum liquid fluidization velocity was calculated as the average of the transition velocities obtained from the standard deviation, average frequency, high frequency Hurst exponent, and the V statistic of the cross-sectional average

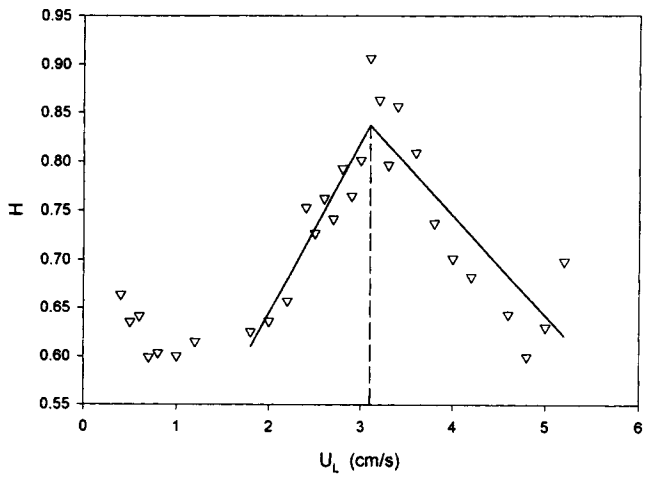

Figure 14. High-frequency Hurst exponent of the cross-sectional average conductivity signal at a superficial gas velocity of 1.7 cm/s.

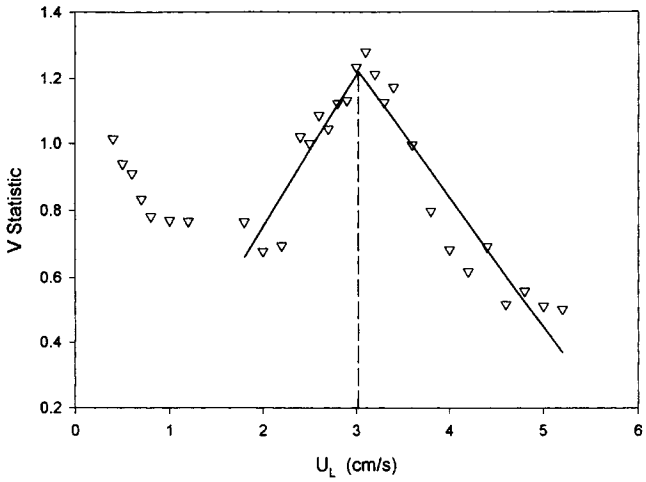

Figure 15. Maximum V statistic of the cross-sectional average conductivity signal at a superficial gas velocity of 1.7 cm/s.

conductivity signal. The minimum liquid fluidization velocity decreased with the introduction of gas (Figure 16). At higher gas velocities, between 8 and 12 cm/s, the minimum liquid fluidization velocity becomes approximately constant at 1.8 cm/s. Figure 16 shows, for each gas velocity, that the bed was in the agitated regime over a significant range of liquid velocities. Comparison with Figure 1 shows that the minimum fluidization velocities measured in this study are within the wide range of values predicted from literature correlations.

Conclusions

A gas-liquid-solid system of 3 mm glass beads exhibits three distinct flow regimes as the liquid velocity is increased: the compacted, agitated, and fluidized regimes. The bed is not fluidized in the agitated bed regime.

Pressure gradient measurement, a standard technique, and bed expansion do not provide the minimum liquid fluidization velocity, but, rather, the velocity between the compacted and agitated bed regimes.

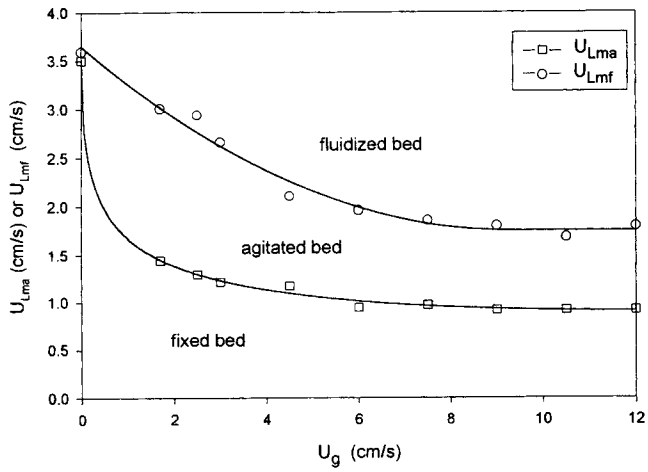

Figure 16. Minimum agitation and minimum liquid fluidization velocity of a gas-liquid-solid system of 3-mm glass beads as a function of superficial gas velocity.

At low superficial gas velocities, it is difficult to determine the minimum liquid fluidization velocity from time-averaged conductivity and bubble probe signals.

The minimum liquid fluidization velocity can be obtained from the standard deviation, the average frequency, the Hurst exponent, and the V statistic of the cross-sectional average conductivity which can be measured under industrial conditions.

The minimum liquid fluidization velocity decreases with the introduction of gas. At the higher gas velocities, between 8 and 12 cm/s, the minimum liquid fluidization velocity of a gas-liquid-solid system of 3 mm glass beads becomes approximately constant at 1.8 cm/s.

Acknowledgments

The authors gratefully acknowledge the Natural Sciences and Engineering Research Council (NSERC) of Canada for their financial support in the form of a Scholarship to L. A. Briens and an Operating Research Grant to C. L. Briens. The authors thank Dr. C. Hudson for contribution of the bubble probe. The authors also wish to thank V. P. Briens for keeping them to the bare facts.

Literature Cited

Begovich, J. M., and J. S. Watson, "Hydrodynamic Characteristics of Three-Phase Fluidized Beds," *Fluidization*, J. F. Davidson and D. L. Kearins, eds., Cambridge Univ. Press, Cambridge, UK, p. 190 (1978).

Briens, C. L., L. A. Briens, J. Hay, C. Hudson, and A. Margaritis, "Application of Hurst Analysis to the Detection of Minimum Fluidization and Gas Maldistribution in Gas-Liquid-Solid Fluidized Beds," *AIChE J.*, in press (1997).

Costa, E., A. de Lucas, and P. Garcia, "Fluid Dynamics of Gas-Liqud-Solid Fluidized Beds," *Ind. Eng. Chem. Process Des. Dev.*, **25**, 849 (1986).

Dullien, F. A. L., "Structural Properties of Packings of Particles," *Handbook of Powder Science and Technology*, M. E. Fayed and L. Otten, eds., van Nostrand Reinhold, New York, p. 99 (1984).

Ermakova, A., G. K. Ziganshin, and M. G. Slin'ko, "Hydrodynamics of a Gas-Liquid Reactor with a Fluidized Bed of Solid Matter," *Theor. Found. Chem. Eng.*, **4**, 84 (1970).

Fan, L.-S., *Gas-Liquid-Solid Fluidization Engineering*, Butterworth, Boston (1989).

Fortin, Y., "Reacteurs à Lit Fluidisé Triphasique: Caractèristiques Hydrodynamiques et Mélange des Particles Solides," PhD Thesis, Ecole Nationale Superiéure du Pétrole et des Moteurs, France (1984).

Grace, J. R., "Fluidized-Bed Hydrodynamics," *Handbook of Multiphase Systems*, G. Hetsroni, ed., McGraw-Hill, New York, p. 8 (1982).

Hudson, C., "Effect of Inclination on Hydrodynamics and Heat Transfer in Bubble Columns, Liquid-Solid, and Gas-Liquid-Solid Fluidized Beds," PhD Thesis, Univ. of Western Ontario, London, Canada (1996).

Hurst, H. E., "Methods of Using Long-Term Storage in Reservoirs," *Trans. ASCE*, **116**, 770 (1951).

Jean, R.-H., "Hydrodynamics and Gas-Liquid Mass Transfer in Liquid-Solid and Gas-Liquid-Solid Fluidized Beds," PhD Thesis, Ohio State Univ., Columbus (1988).

Lee, J. C., and N. Al-Dabbagh, "Three-Phase Fluidized Beds. Onset of Fluidization at High Gas Rates," *Fluidization*, J. F. Davidson and D. L. Kearins, eds., Cambridge University Press, Cambridge, UK, p. 184 (1978).

Merchant, F. J. A., A. Margaritis, and J. B. Wallace, "A Novel Technique for Measuring Solute Diffusivities in Entrapment Matrices Used in Immobilization," *Biotech. Bioeng.*, **30**, 936 (1987).

Nacef, S., "Hydrodynamique des Lits Fluidisés Gaz-Liquide-Solide: Effets du Distributeur et de la Nature du Liquide," PhD Thesis, Institut National Polytechnique de Lorraine, Ecole Nationale Supérieure des Industries Chimiques de Nancy, France (1991).
Nacef, S., G. Wild, A. Laurent, and S. D. Kim, "Effects d'Échelle en Fluidisation Gaz-Liquide-Solide," *Entropie*, **143–144**, 83 (1988).
Nowak, W., M. Hasatani, and M. Derczynski, "Fluidization and Heat Transfer of Fine Particles in an Acoustic Field," *AIChE Symp. Ser.*, **296**, 137 (1993).
Saberian-Broudjenni, M., G. Wild, J.-C. Charpentier, Y. Fortin, J.-P. Euzen, and R. Patoux, "Contribution to the Hydrodynamic Study of Gas-Liquid-Solid Fluidized-Bed Reactors," *Int. Chem. Eng.*, **27**, 423 (1987).
Saberian-Broudjenni, M., G. Wild, and J. C. Charpentier, "The Minimum Fluidization Velocity in Gas-Liquid-Solid Fluidization," *Frontiers in Chemical Reaction Engineering*, Vol. 1, L. K. Doraiswamy and R. A. Mashelkar, eds., Wiley Eastern, New Dehli, p. 405 (1984).
Song, G. H., F. Bavarian, and L.-S. Fan, "Hydrodynamics of Three-Phase Fluidized Bed Containing Cylindrical Hydrotreating Catalysts," *Can. J. Chem. Eng.*, **67**, 265 (1989).
Zhang, J.-P., N. Epstein, J. R. Grace, and J. Zhu, "Minimum Fluidization Velocity of Gas-Liquid Fluidized Beds," *Trans. IChemE*, **73**, 347 (1995).

Manuscript received May 28, 1996, and revision received Sept. 4, 1996.

Corrections

• In the article titled "Nonlinear Control of High-Purity Distillation Column Using a Traveling-Wave Model" (March 1997, p. 703), the original version of Figure 7 was published. The correct Figure 7 is:

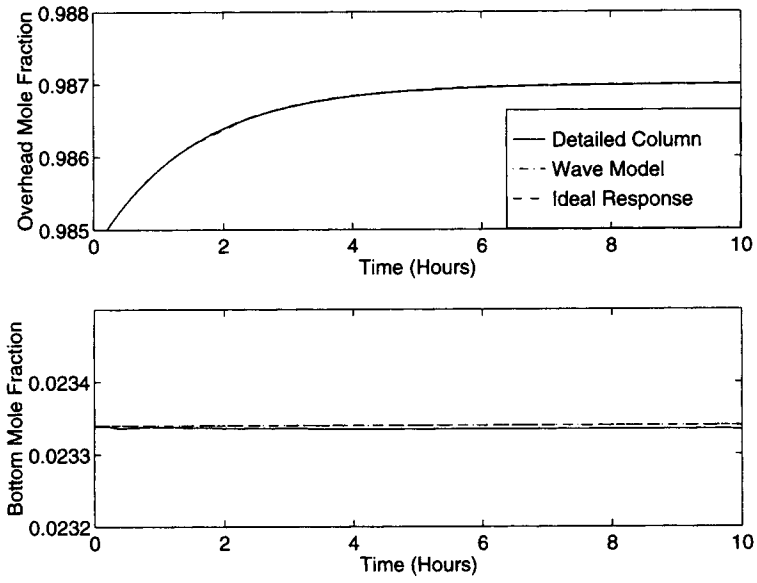

Figure 7. Open-loop step change of +0.02 in the transformed input v_1 keeping v_2 constant shows linear, decoupled response.

• In the article titled "Phase-Change Heat Regenerators: Modeling and Experimental Studies" (March, 1996, p. 791), the ratio of the terms ϵ_B and ψ in Eq. 2 should be inverted, i.e., ϵ_B should be in the numerator rather than the denominator and ψ in the denominator rather than the numerator. In the same equation, the second subscript, l, on the second μ term should be a c. Thus, Eq. 2 should read as

$$\mu_{s,h} = \mu_{s,c} = (1+\psi)\frac{L\epsilon_B}{v_f\psi} \tag{2}$$

In addition, the first line of text on p. 794, the term "m^3 bed-" was omitted. The corrected line should read: "where ϵ_B is the bed porosity [(m^3 bed-m^3 packing)/m^3 bed], ρ_f and". The definition as it appeared in the text is equal to the term $(1-\epsilon_B)$, not the bed porosity and, hence, prone to generate confusion.

The above errors do not affect the other equations or findings of this work.